Analytically-Guided Design of a Tailed Bipedal Hopping Robot

Abdulaziz Shamsah* Avik De† Daniel E. Koditschek†

***Abstract*— We present the first fully spatial hopping gait of a 12 DoF tailed biped driven by only 4 actuators. The control of this physical machine is built up from parallel compositions of controllers for progressively higher DoF extensions of a simple 2 DoF, 1 actuator template. These template dynamics are still not themselves integrable, but a new hybrid averaging analysis yields a conjectured closed form representation of the approximate hopping limit cycle as a function of its physical and control parameters. The resulting insight into the role of the machine's kinematic and dynamical design choices affords a redesign leading to the newly achieved behavior.**

I. Introduction

We present empirical evidence for the efficacy of an emerging parallel composition formalism [2, 3] applicable to hybrid systems [4] of the sort arising in robots that rely upon energetic exercise of their appendages to achieve both propulsion and stabilization. We rework the Jerboa tailed biped [1] and demonstrate for the first time a fully spatial hopping bipedal machine (still-shot-captured in Fig. 1) whose pronounced kinematic asymmetries simultaneously confer a diverse array of steady state and transitional behaviors [5] while at the same time challenging the intuitive leap from kinematic to dynamical symmetry that has guided legged robotics since its pioneering articulation by Raibert [6]. By conjecturing (but not yet proving) the hybrid averageability [7] of a (kinematically highly asymmetric) 2 DoF template—the "Tailed Vertical Hopper" (TVH) depicted in Fig. 2(a)—we obtain an analytically exact representation of the putative manner in which its physical and control parameters determine its steady state behavior. This affords a principled redesign of the Jerboa legs and tail so as to promote the parallel composition of a succession of additional controllers targeting more and more of the physical machine's true DoF (depicted in Fig. 2(b,c,d)) in a manner that (we conjecture) stably anchors the simple template [8] with no need for overt symmetry in either kinematic or dynamical parameters. This paper describes the salient aspects of this redesign and offers empirical evidence supporting our conjectured explanation for the success of the novel behavior illustrated in Fig. 1.

A. Motivation and Related Work

1) Bioinspiration for tails: Tailed locomotion is widely studied in animals whose tails are known to adjust shape during flight [9], stance [10], and for reorientation [11]. Bioinspired robot designs often introduce a tail (i.e. an appendage that exerts high inertia on the robot body but does not effect the location of center of mass [12]), to reorient during flight [13–15]. Robotic tails have also been used to assist in leaping [5]. To the best of the authors' knowledge, the Penn Jerboa [1] is the first robot to have used its tail to energize hopping as well as for balance and attitude control [2, 16]. These varied uses for tails suggest their broader value in affording many different behaviors with relatively few actuators, thereby allowing for high power density.

2) Robot locomotion performance: While locomotion-targeted robot design studies often focus on the isolated optimization of key components like actuators [17] or gearboxes [18], or both simultaneously [19], fewer attempts have been made to trace the benefits forward to overall platform performance [15, 20–22].

B. Claims and Organization

The novelty of our contribution (compared to aforementioned prior work) is that: (a) we use the tail as not just a reorientation device [15], but also in the relatively unusual role of a primary energy source [2]; and (b) analytical intractability of the hybrid limit cycles—whose fixed points and linearizations we seek to tune—heretofore precluded the closed form exploration of the large space of design and control parameters in all but low DoF settings.

Specifically, in this paper, we take initial steps toward a formal morphological reduction [23] of the 4 actuator, 12 DoF Jerboa robot onto the 1 actuator, 2 DoF TVH template by using hybrid averaging [7, 24] to project the large and unintuitive[1] parameter space of the Jerboa onto its equilibrium hopping height, our candidate metric of hopping performance (13). In so doing, we (a) enable selection of control gains for metrically accurate hopping height control (Fig. 4), (b) establish that leg damping on the Jerboa is not just energetically wasteful, but limits hopping performance even without any limits on available actuator force/power. Consequent to (a), we show empirically that this enhancement in controlled vertical hopping (Fig. 6) promotes far more accurate planar hopping performance[2] than demonstrated before (Fig. 8–11) [2], and enables this machine's first forays into spatial hopping (Fig. 1, 12). Consequent to (b), we revise the Jerboa leg design with COTS materials and the guidance of newly-introduced leg-design metrics in order to minimize both

*Mechanical Engineering and Applied Mechanics, †Electrical and Systems Engineering, University of Pennsylvania, Philadelphia, PA, USA. {shamsah,avik,kod}@seas.upenn.edu.

This work was supported in part by AFRL grant FA865015D1845 (subcontract 669737-1) and in part by ONR grant #N00014-16-1-2817, a Vannevar Bush Fellowship held by the last author, sponsored by the Basic Research Office of the Assistant Secretary of Defense for Research and Engineering.

[1]For example, as discussed in [1], it is not intuitively clear how changing tail mass (m_t in Fig. 2) affects hopping performance.

[2]with tracking accuracy reduced somewhat by various error sources which we discuss in Sec. IV-E.

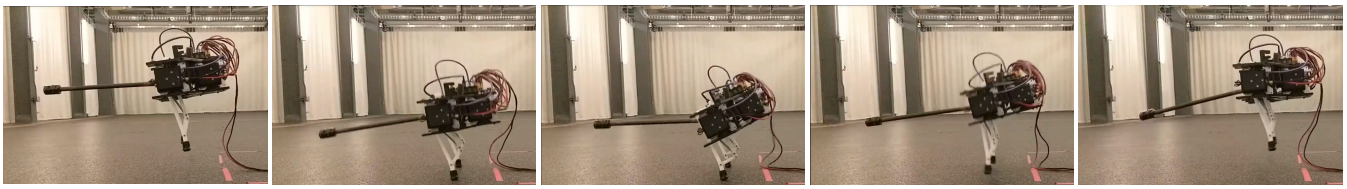

Fig. 1. Storyboard snapshots of unconstrained spatial hopping with the Penn Jerboa [1]: a 12 DoF tailed bipedal robot driven by only 4 actuators.

damping, and the presence of coupling between radial and tangential forces acting through the leg (Sec. III).

Sec. II presents an analytical investigation of the TVH template (Fig. 2(a)), an approximate model (Assumption 1) of tailed vertical hopping which exposes the parameters that are analytically relevant to tailed hopping performance. Fig. 4 compares these analytical predictions against both numerical and empirical data, showing that the saturation effects (and their relation to the system parameters) predicted by the analysis are borne out in the physical world.

Sec. III leverages these analytical suggestions and shows how to implement changes in the mechanical design of the robot to obtain better performance than possible before [2].

In Sec. IV we build upon the analytically-founded improved height-tracking performance in a tailed vertical hopper (Fig. 4–6) by empirically deploying it on progressively higher DoF anchors (physical models of increasingly realistic complexity [8]) (Fig. 2). We demonstrate that our analytically-guided design-and-control improvements enable superior hopping performance than in past work.

In Sec. V, we present our conclusions, and future work.

II. Tailed Vertical Hopping (2DOF) Analysis

In [7], we introduced an analytical tool for ε-perturbation stability analysis of hybrid limit cycles.[3]

A key insight is to leverage the perturbation parameter $\varepsilon > 0$ in order to analytically study the effects of feedback control parameters as well as mechanical design parameters, on the fixed point (as we do in this paper) or the stability properties of the hybrid system [3].

A. Tailed Vertical Hopping Model (TVH, Fig. 2(a))

1) Lagrangian modeling: Based on the model in Fig. 2(a), our configuration variables are $\mathbf{q} := (z, \xi)$. The leg spring has a stiffness $m_b\omega_{\mathrm{v}}^2$. Note that the tail position is

$$p_t := \begin{bmatrix} 0 \\ z \end{bmatrix} + \rho_t \begin{bmatrix} \cos\xi \\ \sin\xi \end{bmatrix}, \tag{1}$$

and the Lagrangian $\mathcal{L} = T - V$ is defined as usual from the physical kinetic and potential energies

$$\begin{aligned} T(\mathbf{q}, \dot{\mathbf{q}}) &= \frac{1}{2} m_b \dot{z}^2 + \frac{1}{2} m_t \dot{p}_t^2, \\ V(\mathbf{q}) &= m_b g z + m_t g e_2^T p_t + \frac{m_b \omega_{\mathrm{v}}^2 (z-\rho)^2}{2}. \end{aligned} \tag{2}$$

To $\ddot{\mathbf{q}}$ we add the crucial damping from the leg shank, which we model as a lumped (mass-normalized[4]) viscous friction force $\varepsilon\beta\dot{z}$, as well as the tail damping, also modeled as a viscous force $\beta_t\dot{\xi}$.

Assumption 1 (Jerboa physical parameters scaling)**.** *For our analysis, we make the following assumptions about the physical parameters:*

a) As in our previous work [2], we assert that the tail is light but has non-negligible inertia, formalized here by scaling the physical tail mass m_t and tail length ρ_t by the non-dimensional scale parameter ε as

$$m_t = \varepsilon^2 \widetilde{m}_t \qquad \rho_t = \widetilde{\rho}_t / \varepsilon. \tag{3}$$

b) We assert that tail has high damping and exhibits generalized damper [25, 26] (first-order) dynamics, and in particular, $\beta_t = \mathcal{O}(\varepsilon^{-1/2})$.

Note that the tail inertia, $i_t = m_t\rho_t^2$ is again independent of ε. In our physical robot (Table I), we used a range of tail masses ranging between 7–10% of the body mass. Additionally, the construction of the tail actuator (with a belt transmission consisting of 3D-printed sprockets [1]) presents a high degree of viscous damping. In comparing a numerical simulation to the empirical data (part of which is presented in Fig. 4), we found[5] that the viscous damping force $\beta_t\dot{\xi} \gg \ddot{\xi} \approx 0$.[6] This places the system in a generalized damper regime, as we have asserted in Assumption 1.

2) Equations of motion: We derive the equations of motion from the Lagrangian and subject to Assumption 1. First, note that the tail dynamics are

$$\ddot{\xi} = \frac{\Upsilon_t}{i_t} + \varepsilon \frac{\omega_{\mathrm{v}}^2 \cos\xi (z-\rho)}{\widetilde{\rho}_t} - \beta_t \dot{\xi}, \tag{4}$$

where we remind the reader that $i_t = m_t\rho_t^2 = \widetilde{m}_t\widetilde{\rho}_t^2$ appears in the Lagrangian through the definition of p_t (1). We simplify further according to Assumption 1 as described above to get

$$\begin{aligned} \ddot{z} &= \omega_{\mathrm{v}}^2(\rho - z) - g - \varepsilon\beta\dot{z} + \varepsilon\Big(\frac{\widetilde{m}_t\widetilde{\rho}_t \sin\xi\dot{\xi}^2}{m_b} - \frac{\Upsilon_t \cos\xi}{m_b\widetilde{\rho}_t}\Big) \\ \dot{\xi} &= \frac{\Upsilon_t}{\widetilde{m}_t\widetilde{\rho}_t^2\beta_t} + \frac{\varepsilon\omega_{\mathrm{v}}^2\cos\xi(z-\rho)}{\beta_t\widetilde{\rho}_t}, \end{aligned} \tag{5}$$

where the second equation is obtained by setting $\ddot{\xi} \approx 0$ (Assumption 1) in (4), and $\mathcal{O}(\varepsilon^2)$ and higher terms are dropped. We can see from the $\ddot{z}$ expression how the tail

[3] We omitted the statement of the theoretical result due to lack of space.

[4] I.e., $\varepsilon\beta = b/m_b$, where b is the physical damping constant, in standard units of Ns/m.

[5] For instance, in the numerical trial with "Delrin" parameters in Fig. 4, with $k_{\mathrm{emp}} = 0.5$,

[6] In Fig. 7, we document evidence of this behavior: based on our torque input (7), the resulting tail position and velocity traces are "in phase" with our damper-based prediction in (9) (position) and (5) (velocity).

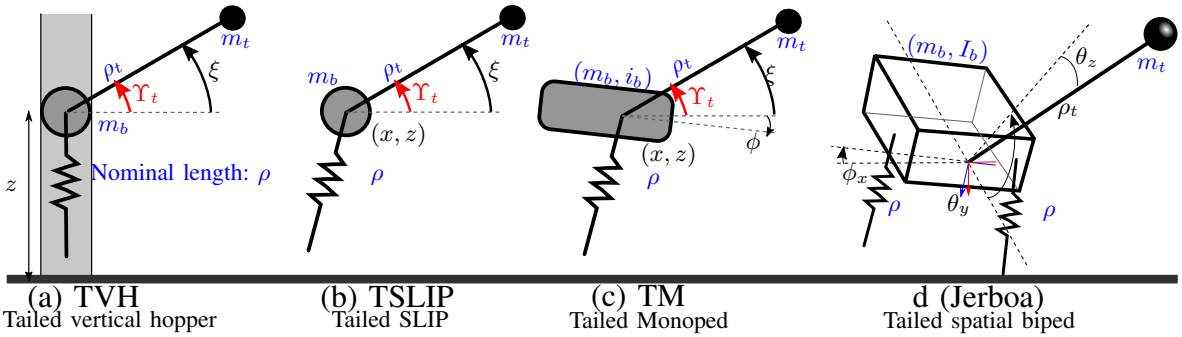

Fig. 2. Even though our analysis (Sec. II) only provides insight into vertical hopping, our experimental results in this paper explore the behavior of each one of the increasingly higher DOF systems depicted here: the 2DOF TVH (Fig. 4, 6 & 7); the 3DOF TSLIP (Fig. 8 & 9); the 4DOF TM (Fig. 10 & 11); and the fully spatial Jerboa (Fig. 12).

torque Υ_t and the tail state $\xi, \dot{\xi}$ couple into the vertical acceleration. We also define a new symbol for the $\mathcal{O}(\varepsilon)$ terms in the $\ddot{z}$ expression in (5)),

$$\nu_{\mathsf{v}} := \frac{\widetilde{m}_t \widetilde{\rho}_t \sin\xi \dot{\xi}^2}{m_b} - \frac{\Upsilon_t \cos\xi}{m_b \widetilde{\rho}_t} - \beta a_{\mathsf{v}} \sin\psi_{\mathsf{v}}. \tag{6}$$

B. Closed Loop TVH Dynamics

1) Tail controller: In the 2DOF system here, we only have a single input: Υ_t. We use the previously-introduced [2] phase-locked tail-energy-pumping controller

$$\Upsilon_t := -k \sin\psi_{\mathsf{v}}. \tag{7}$$

2) Candidate averageable coordinates: We use the vertical hopper template from [27] to define $(a_{\mathsf{v}}, \psi_{\mathsf{v}})$ from the physical $(z, \dot{z})$ coordinates

$$(\rho - z)\omega_{\mathsf{v}} = a_{\mathsf{v}} \cos\psi_{\mathsf{v}}, \qquad \dot{z} = a_{\mathsf{v}} \sin\psi_{\mathsf{v}}, \tag{8}$$

with the goal of obtaining a pair of slow (a_{v}) and fast (ψ_{v}) coordinates useful for averaging.[7] In this instance, a_{v} is the square root of the mechanical energy of the oscillating mass (with slow dynamics), while ψ_{v} is a phase coordinate increasing through stance (with fast dynamics).

We introduce a new coordinate change for the single tail state ξ, which leverages the special structure[8] of the leg-phase-locked tail energization (7),

$$\begin{aligned} a_{\mathsf{t}} &:= \xi - \xi_0 - \Xi \cos\psi_{\mathsf{v}}, \text{ where} \\ \Xi &:= \frac{k}{i_t \beta_t \omega_{\mathsf{v}}}. \end{aligned} \tag{9}$$

where ξ_0 is the tail reset angle. We provide an intuitive interpretation of Ξ below (12). Note that Ξ is a non-dimensional constant, since the units of k [N], i_t [kg-m^2], β_t [s^{-1}], and ω_{v} [s^{-1}] cancel.

[7]The inverse coordinate change (from physical to averageable coordinates) is then $a_{\mathsf{v}}^2 = ((\rho - z)\omega_{\mathsf{v}})^2 + \dot{z}^2$, and $\tan\psi_{\mathsf{v}} = \frac{\dot{z}}{(\rho - z)\omega_{\mathsf{v}}}$.

[8]Note from (5) that $\dot{\xi}$ is strongly coupled to the vertical dynamics through our tail control (7), and rather more weakly to ξ itself, motivating the introduction of ψ_{v} into the definition of a_{t} below (9).

3) Closed-loop dynamics in averageable coordinates: In (7), we have explicitly set Υ_t to be a function of the vertical z coordinates. The closed-loop vertical dynamics are then (similar to the vertical hopper template in [27], with ν_{v} defined in (6)),

$$\dot{a}_{\mathsf{v}} = \varepsilon \sin\psi_{\mathsf{v}} \nu_{\mathsf{v}}, \qquad \dot{\psi}_{\mathsf{v}} = \omega_{\mathsf{v}} + \varepsilon \cos\psi_{\mathsf{v}} \nu_{\mathsf{v}}. \tag{10}$$

For the tail variable, using the definitions above and (5), (7), and (10) we get

$$\dot{a}_{\mathsf{t}} = \varepsilon \Big(\frac{k \nu_{\mathsf{v}} \cos\psi_{\mathsf{v}} \sin\psi_{\mathsf{v}}}{i_t \beta_t \omega_{\mathsf{v}}} - \frac{\omega_{\mathsf{v}}^3 a_{\mathsf{v}} \cos\xi \cos\psi_{\mathsf{v}}}{\beta_t \widetilde{\rho}_t} \Big) + \mathcal{O}(\varepsilon^2), \tag{11}$$

In these coordinates, we get the averageable vector field in the coordinates $\sigma = \psi_{\mathsf{v}}$, $\mathbf{x} = (a_{\mathsf{v}}, a_{\mathsf{t}})$,

$$\begin{aligned} \dot{\mathbf{x}} &= \varepsilon f(\mathbf{x}, \sigma, \varepsilon) \\ &= \varepsilon \begin{bmatrix} \sin\psi_{\mathsf{v}} \nu_{\mathsf{v}} \\ \frac{k \nu_{\mathsf{v}} \cos\psi_{\mathsf{v}} \sin\psi_{\mathsf{v}}}{i_t \beta_t \omega_{\mathsf{v}}} - \frac{\omega_{\mathsf{v}}^3 a_{\mathsf{v}} \cos\xi \cos\psi_{\mathsf{v}}}{\beta_t \widetilde{\rho}_t} \end{bmatrix} + \mathcal{O}(\varepsilon^2), \end{aligned} \tag{12}$$

with period $T = \pi$.

Note that our definition of a_{t}—and its consequent slow dynamics as shown in (11)—ensures that it is roughly constant through stance, and in addition, note that at touchdown (beginning of stance), $\psi_{\mathsf{v}}(t_{\mathrm{TD}}) = -\pi/2$ (from (8), setting $z = \rho$), and so $\xi = \xi_0 \iff a_{\mathsf{t}}(t_{\mathrm{TD}}) = 0$. Consequently, we see that from (9), Ξ is in fact the tail amplitude in radians. In Fig. 4, we compare Ξ to numerical and empirical tail amplitudes obtained from the original system (Fig. 2(a)) without Assumption 1. Note that we allow the ξ_0 constant to be chosen ahead of time to ensure the tail does not intersect the ground at the beginning of stance.

4) Approximate equilibrium hopping height: Since the focus of this paper is on analytically-guided design, we don't pursue a full averaging stability analysis here. We only seek an expression for an approximation of the equilibrium orbit (below). We leave as conjecture the following:

Conjecture 1. *The TVH system is averageable (in the sense of [7]), and the averaged system is stable.*

In this paper we are interested in an expression for the equilibrium hopping height, or equivalently, a_{v}^*. To this end,

we compute the first element of the averaged vector field $\overline{f}$:

$$e_1^T \overline{f}(\mathbf{x}) = \frac{e_1^T}{\pi} \int_{-\pi/2}^{\pi/2} f(\mathbf{x}, \sigma, 0) d\sigma$$
$$= \frac{-a_{\mathrm{v}}\beta}{2} + \frac{\widetilde{m}_t \beta_t \widetilde{\rho}_t \omega_{\mathrm{v}}}{m_b} (J_1(\Xi)\cos\xi_0 - \sin\xi_0 H_1(\Xi)),$$

where $J_1 : \mathbb{R} \to \mathbb{R}$ is the Bessel function of the first kind, and $H_1 : \mathbb{R} \to \mathbb{R}$ is the Struve function [28]. Solving for a root of this expression, we see that the (averaged) equilibrium is located at

$$a_{\mathrm{v}}^* = \frac{2\widetilde{m}_t \beta_t \widetilde{\rho}_t \omega_{\mathrm{v}}}{m_b \beta} (J_1(\Xi)\cos\xi_0 - \sin\xi_0 H_1(\Xi)), \qquad (13)$$

which depends on both physical $(m_b, \widetilde{m}_t, \widetilde{\rho}_t, \omega_{\mathrm{v}}^2, \beta)$ and controller (k) parameters.

5) Implications for Jerboa design and hopping performance: We now summarize the insights gained in this section relating TVH system parameters to its performance.

a) Vertical energization saturates due to the mechanics: Another instance in which we have used a similar vertical energization strategy is in a quadruped robot with actuated leg shank [3]. However, in the Jerboa, there is no shank actuator, and in addition to joint torque limits, there is an energization limit imposed by the nature of the tail coupling in (5): intuitively, with finite tail torque Υ_t, as the tail approaches vertical ($\cos\xi \to 0$), our affordance on $\ddot{z}$ vanishes. We see this "saturation" in numerical as well as empirical[9] trials in Fig. 4: intuitively, toward the left of the figure, increasing tail gain k allows us to select higher hopping heights, but after a point, further increases in k force the tail angle to be more vertical for a larger portion of stance (9), thus diminishing our ability to access still-higher hopping height setpoints.

b) Metrically accurate height setpoint tracking: The parenthesized term on the right hand side of (13) depends only on our control gain k, and constant parameters. The selection of appropriate k may be further limited by kinematic workspace, which we do not model in this paper. Numerical methods acting on (13) can reveal an "inverse map" from desired hopping height to appropriate tail gain (e.g. Fig. 4), despite the non-integrable return map of the TVH system (Fig. 2(a)).

III. Design Implementation

We iterate on the prior design of the Penn Jerboa [1] with the goal of addressing the design deficiencies that have thus far precluded full spatial operation.

A. General Design Changes

In Table I, we tabulate the quantitative differences between the revised platform (Fig. 1) and the prior one, and we have discussed the relation of the parameters to our analytical assumptions just below Assumption 1.

1) We have increased the non-dimensional roll inertia for improved preflexive roll stability [3]. We achieve this by widening the body and placing the leg actuators at the outside edges of the body.
2) We incorporated a more accurate IMU (VN-100) [29], which helps significantly in pitch stabilization in 4DOF planar hopping.
3) We introduced a magnetic encoder attached to each leg "extension" joint (Fig. 3) that measures the leg extension. This measurement is used to calculate ψ_{v} for oscillatory tail energization (7), as well as for touchdown detection (formerly achieved using an IR distance sensor [16]). This measurement also allows for on-line calculation of the leg infinitesimal kinematics, which we can subsequently use to estimate the fore-aft body velocity.[10]
4) The robot also uses commercial motor modules [30] for easier calibration. Unfortunately, the new motor modules and the larger body increase the mass of the platform relative to the previous design. (Table I).
5) We have incorporated a 5° leg splay angle to help with passive roll stability based on findings in [31].

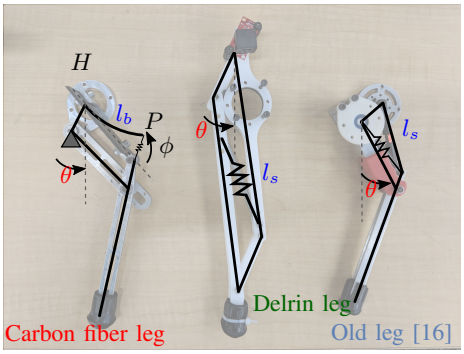

Fig. 3. Candidate leg designs evaluated in this paper, showing the location of the compliance DOF (blue), and the actuated DOF (red).

TABLE I
New and Old Jerboa Design Parameters

	New Design	Old Design [16]
Weight (Kg)	2.770	2.419 (With Battery)
Dimensions (cm)	22(L)x37(W)x9(H)	21(L)x22(W)x10(H)
Tail Length (cm)	40	40
Tail Mass (g)	270 (TVH, TSLIP) 190 (TM, Jerboa)	150

B. Leg Design

The design of the leg (modeled as a prismatic passive spring, and actively-controlled revolute hip joint) plays an important role in decoupling the radial and tangential reaction forces in fore-aft hopping. Many designs were historically considered in the design of the Jerboa leg [1, 16], but the analytical result of Sec. II motivates a new study in this area. This paper revisits the leg design study for RHex in [20], with the following distinctions: with a focus

[9]The empirical trials suffer in addition (but to a smaller extent) from flux saturation in the motors [1], which is beyond the scope of our modeling.

[10]As in [2], we use a Raibert-inspired "neutral point" controller [6] for fore-aft speed control (without proof).

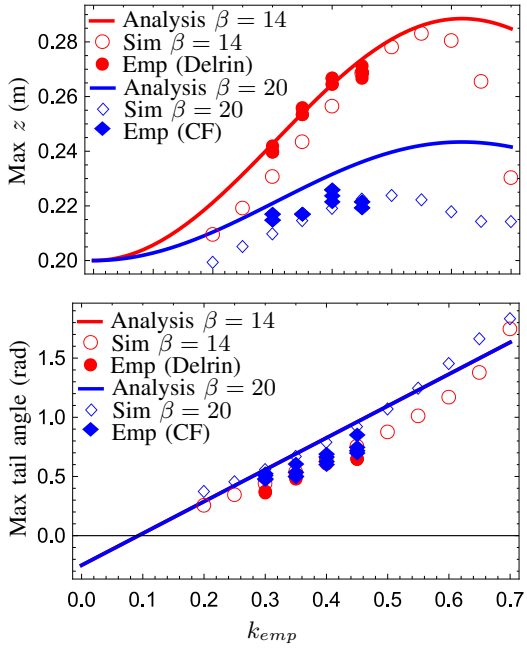

Fig. 4. A comparison of our analytical prediction (13) (solid line) to numerical (hollow markers) and empirical data (solid markers). The physical parameters m_t, ρ_t were substituted with their measured values, but damping parameters $\beta = 14s^{-1}, \beta_t = 20s^{-1}$ were approximately tuned to fit the numerical trials to empirical data.

on easier manufacturability, we only consider off-the-shelf materials, and no composites with custom layups. In addition we introduce a new metric related to the decoupling of radial and tangential forces acting on the leg (below).

1) Candidate designs: The models for all three legs considered in this study are shown in Fig. 3 and include

- **Previously used leg [16]**
- **Carbon fiber (CF) leaf spring.** The carbon fiber leaf is modeled as a cantilever beam as shown in Fig. 3, where $l_s = \frac{3l_b\phi}{2}$. To simplify the kinematics, we assume a small angle of deflection ϕ, so that the distance between hip H and the secondary attachment point P remains constant and $\approx l_b$ (Fig. 3). In [20], the authors empirically measured the resultant forces at the toe, to help model a similar leaf-spring design as a combination of rigid bodies and rotational springs, whereas our model is more similar to the way ATRIAS legs are modeled in [32].
- **Delrin 4-bar with extension spring.** The leg consists of two layers of delrin, with a gap between them, where the spring is attached to shafts supported symmetrically on either side. A similar design was explored in the original iteration of Jerboa [1], but not employed for empirical trials.

2) Evaluation criteria: Letting the leg kinematics be defined by $p = g(q)$, where $q = (\ell_s, \theta)$ are the joint coordinates, note that the force applied at the toe from a joint torque vector τ is $\mathrm{D}g^{-T}\tau$. We propose the following criteria for evaluation.

TABLE II
CHARACTERIZATION OF LEG DESIGNS

	Delrin	CF	[16]
Damping b (Ns/m)	20	35	-
Normalized damping β (Ns/m/kg)	7.14	12.5	-
Weight of a single leg (g)	95	96	103
Average γ°	19.08	7.07	33.17
Average α°	69.85	90.69	105.20

a) Reduction of energetic losses (compared to the prior leg [16]): We employ a two-pronged approach:

1) Minimizing joint friction: In the carbon fiber design we use bearings in all joints with sufficient spacing between each link to assure smooth rotation. In the 4-bar design, we specifically use Delrin due to its low friction surface.
2) Preventing bottoming out leg deflection: we avoid using compression springs.

To evaluate energetic losses, we dropped the Jerboa from a fixed height (with quiescent tail) as if the assembly were a simple vertical mass/spring system. We fit the collected data against a linear spring-mass-damper Simulink simulation, where the spring constant and viscous damping (k, b), were adjusted to fit the k, b parameters (See Table II). Note that the damping constant b empirically found here is related to the mass-normalized β in Sec. II as $\beta = b/m_b$.

b) Mitigation of radial/tangential coupling: Recalling our specific goal of parallel composition, coupling of radial (spring) and tangential (hip actuator) forces during stance contributes greatly to anecdotal empirical difficulties [2] in controlling fore-aft speed. Though fore-aft speed control is not the key focus of this paper, our empirical goals (Fig. 8–12) necessitated a further investigation.

There is a large prior body of literature of quantifiable leg design kinematics metrics [20, 33]; but here we devise metrics with our specific decoupling goals in mind:

1) $\gamma := \angle(g(r,\theta), \mathrm{D}g^{-T}e_1)dr$ (smaller better; a pure spring force is as close to radial as possible)[11]
2) $\alpha := e_1^T \mathrm{D}g^{-1}\mathrm{D}g^{-T}e_2 dr$ (smaller better; the columns of the inverse Jacobian are as orthogonal as possible).

By defining the kinematics as explained previously in this section, we plot γ against radial deflection for all three leg designs (Fig. 5), and tabulate the average of γ over the workspace in Table II. The previously used leg [16] had the highest averaged γ of 33.1°, while the CF leg performed the best of all three designs with an average γ of 7.07°.

By plotting α for all three leg designs (Fig. 5), we see that in the leg previously used, α is rarely orthogonal during stance. The CF leg has the best decoupling of radial/tangential forces, with maximum deviation from orthogonality of $\approx 20°$. The Delrin design deviates significantly from orthogonality, however at maximum spring deflection (the point at which the radial force is the largest), α is close to orthogonality with only $\approx 15°$ deviation. The averages of α over stance are summarized in Table II.

[11]This measure is evocative of a similar measure in [20, Sec. 3.3], but the characterization was qualitative. Our quantitative results are in Table II.

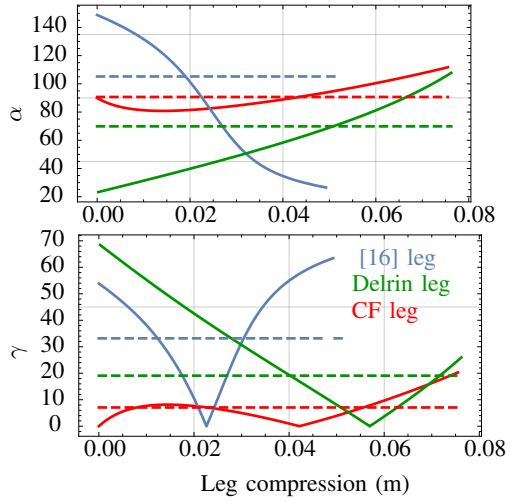

Fig. 5. Comparison of candidate leg designs using our criteria described in Sec. III-B.2. The dashed line is the workspace-average in each case.

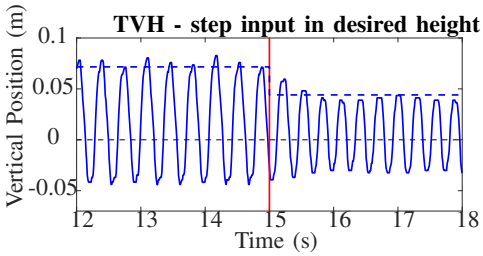

Fig. 6. A sequence of step inputs of desired height (commanded using a sequence of k_{emp}, in order, 0.45, 0.3). The dashed blue line shows the reference, and the dashed black line is the height at which the legs touch down. Compared to the steady-state tracking presented in Fig. 4, the requisite "settling time" of around 3 hops is visible in this plot.

3) Conclusion: While the CF design outperformed the 4-bar delrin design in mitigating the radial/tangential coupling, its viscous damping is unacceptably high. Therefore, in all future experiments, we use the Delrin leg.

IV. Results

Our empirical results below demonstrate that insight from the TVH analytical study (Sec. II) and improvements in robot design (Sec. III) advance hopping performance for each of the succession of models in Fig. 2 beyond [2]. The robot platform used in these trials is pictured in Fig. 1, and its physical parameters are in Table I. For the data presented in Sec. IV-A–IV-C, we measure height using an instrumented boom, and in Sec. IV-D, from a Vicon motion capture system. We speculate on our sources of error and discrepancy between analytical prediction and empirical outcome in Sec. IV-E.

A. TVH Hopping (2DOF; Fig. 2(a))

In these trials, the robot is attached to the boom with both pitch and horizontal movement locked, constraining the system to vertical hopping (Fig. 2(a)).

To compare the numerical and empirically-found hopping heights to our analytical prediction, in Fig. 4 the hopping height is shown as a function of tail gain k (7). We discuss sources of error in Sec. IV-E.

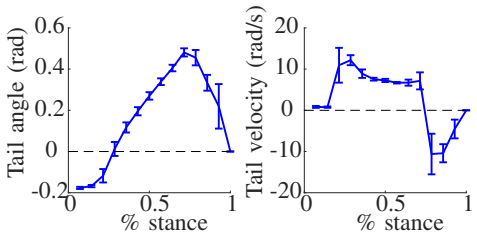

Fig. 7. The tail profile observed during TVH trials (averaged over several stances), showing the cosinusoidal and sinusoidal profiles of the tail position and velocity (respectively), which supports our "generalized damper" assumption in Assumption 1.

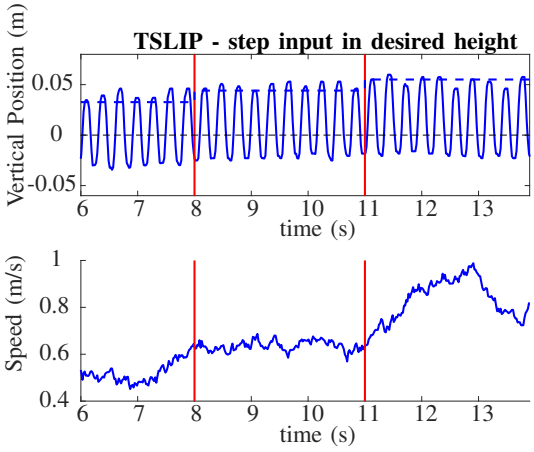

Fig. 8. A sequence of step inputs of desired height. The dashed blue line shows the reference. The dashed black line is the ground. The vertical red lines show were the step input is commanded. In the bottom plot, the velocity is measured using the boom.

We can command hopping height (Fig. 6) as a succession of step inputs of different tail-gain combinations (which correspond to desired height setpoints using (13)).

B. TSLIP Hopping (3DOF; Fig. 2(b))

The robot is attached to the boom with the pitch locked, allowing for free fore-aft motion. In composition with the tail-energization control (7), we instantiate in parallel Raibert's neutral point stepping controller [6], as previously presented in [2], using the hip actuators to position the toe in flight. The introduction of the encoder on the leg joint allows for a superior neutral point estimate than before [2].

While our analytical predictions only pertain to the TVH, we can demonstrate an ability to track TSLIP hopping height in the presence of significant disturbances due to fore-aft motion (Fig. 8).

We show in Fig. 9 our ability to control the speed and stabilize it in relation to a desired reference input. We are also able to stabilize the speed in the face of velocity disturbances added by manually pushing the boom (Included in the video attachment). Combining the ability to control speed and hopping height allows the exploration of more useful hopping behaviors, such as jumping over obstacles that are $6\text{cm} \approx 1/3$ leg length, or over gaps that are $8\text{cm} \approx 1/2$ leg length (Included in the video attachment)

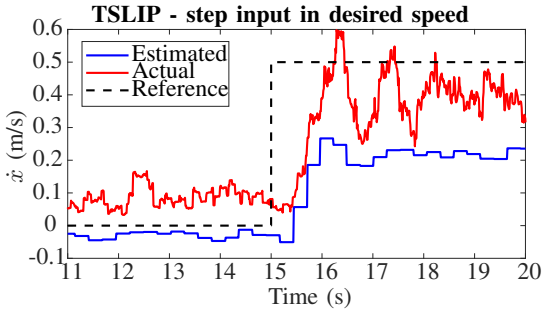

Fig. 9. The estimated speed (blue) is measured through the leg kinematics. whereas the actual speed (red) is measured using the boom.

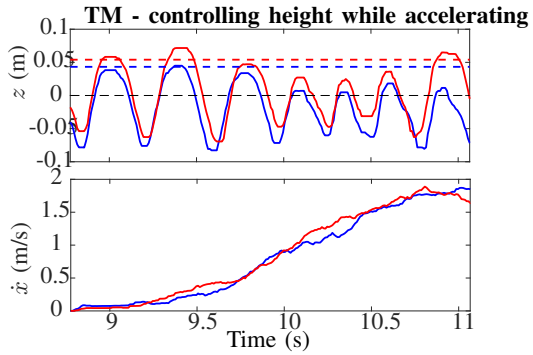

Fig. 10. Two trials with different desired heights. The dashed lines indicate the reference for the trials of the same color. The black dashed line represent the ground. The bottom plots the velocities measured using the boom. The further loss in height-tracking accuracy (relative to the TSLIP anchor (Fig. 8) is due to the introduction of significant cross-talk disturbances arising from attitude and fore-aft energy associated with the accelerating response.

C. TM Hopping (4DOF; Fig. 2(c))

In these tests the robot is attached to the boom with a bearing that allows the robot to pitch freely around its center of mass. In composition with the prior controllers, we use the hip actuator's torque in stance to correct the body pitch in stance, and the tail actuator to control the body-tail "shape" angle, as previously presented in [2]. Fig. 10 shows two trials with two different height setpoints while maintaining almost identical forward velocity. This shows that we are able to control hopping height with limited influence on forward velocity (the goal of our "parallel composition" agenda). Due in part to our design improvements presented here, we can demonstrate the ability to control fore-aft speed (unlike prior work [2]) in Fig. 11. In these trials, the TM repeatedly hopped for up to 20 strides while tracking different reference speeds, before failing due to accumulated speed estimation error (Sec. IV-E).

D. Jerboa Hopping (Unconstrained Spatial; Fig. 2(d))

Now without the boom, we employ in parallel the tailed 2DOF reorientation controller presented in [16], which is responsible for correcting both the body roll angle and the tail yaw angle in flight, using the tail pitch/yaw actuators. In summary, we have composed controllers developed in [2, 16] in parallel: (a) hopping energized by the tail [2]; (b) fore-aft speed control by stepping [2, 6]; (c) hybrid inertial reorientation in flight and stance [2]; (d) frontal-plane tailed reorientation [16]. In these first unconstrained hopping trials, the robot is able to hop for up to 6 strides consistently over several trials (example Fig. 12).

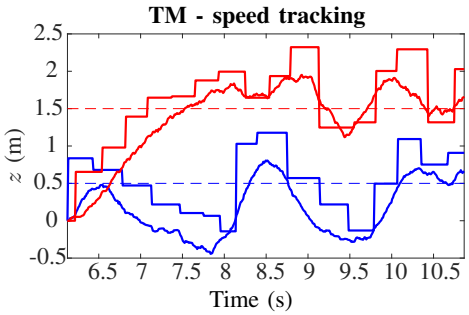

Fig. 11. Two trials that suggest the ability to operate at different speeds in 4DOF. The dashed line indicates the commanded reference. The discrete lines display velocity measurement using leg kinematics during stance, while the continuous traces represent velocity measured using the boom.

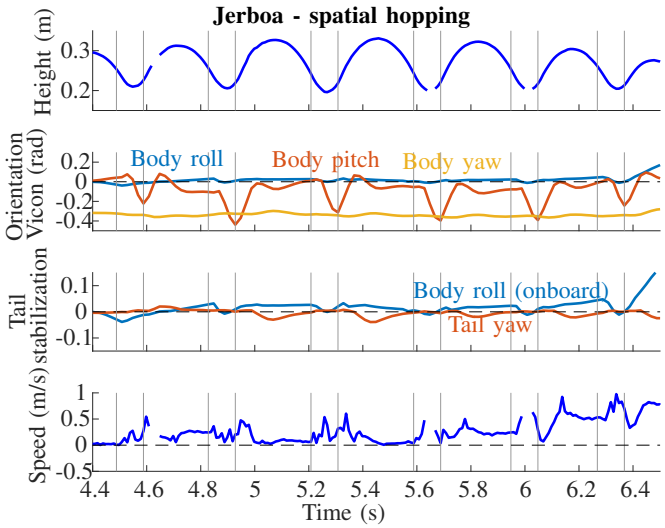

Fig. 12. From top to bottom: Jerboa hopping height recored by VICON; orientation from the onboard IMU; the tail yaw and body roll (demonstrating the activity of the frontal-plane-reorientation controller [16]); and forward velocity recorded by VICON. Although this steady state behavior is not yet robust, we believe that better state estimation and further parameter tuning will afford strongly stable, long duration empirical operation.

E. Sources of Error

In the boom trials, the added mass and inertia of the boom is a significant departure from our model in Fig. 2(a). Our fit for the damping parameters (Fig. 4) includes some contribution from the boom, but the trials including fore-aft motion suffer from further new disturbances.

Tail gains $k_{\text{emp}} > 0.45$ did not result in higher hops (as compared to Fig. 4's somewhat different analytically-predicted saturation). Unmodeled saturating factors on the physical platform include torque limits on the motors, and kinematic range of the leg spring.

In the TM and Jerboa trials, one of the primary failure modes was fore-aft instability. We suspect that the naive "neutral point" approximation [6] is inaccurate in the high-

leg-deflection regime TM / Jerboa operates in. We plan to analyze fore-aft stability more closely in future work in order to rectify that controller. Additionally, our present kinematic speed estimate is updated once per stride (as shown in Fig. 11); its inaccuracy (as compared to the "ground truth") is possibly a significant error source.

In the spatial (Jerboa) trials, accumulated roll error was another failure source—we posit that a larger tail workspace would be beneficial for stabilizing large roll excursions.

V. Conclusion

In this study we introduced an analysis that allowed for some insight into the tuning of unintuitive parameters for tailed vertical hopping. We demonstrated with a large set of empirical trials that such insight allows for improved performance even with a far greater number of unconstrained DOF–even a fully spatial tailed bipedal machine (Fig. 1). To our knowledge, this is the first empirical demonstration of a highly underactuated a tailed hopping robot (4 actuators in total) that is capable of unconstrained spatial hopping.

Future work will be directed toward completing the analysis in Sec. II, and generalizing it to the TSLIP model (Fig . 2(b)). We predict that such analyses will improve our fore-aft speed controller performance (beyond our current ability with Raibert's neutral point algorithm; Fig. 11).

We hypothesize that an analytically-guided approach to design-parameter-tuning (similar to Sec. II) can be generalized to other high DoF platforms, ultimately generalizing the precision of the morphological reduction analysis introduced for a 1 DoF template in [23]. Even though the Jerboa is a specialized machine, inertial coupling between degrees of freedom is used for control in a variety of robotic platforms [23, 34], and an analytical result as in Sec. II-B.5 may help the control designer tune the effectiveness of this sort of coupling at design- or control-time.

References

[1] A. De and D. E. Koditschek, "The Penn Jerboa: A Platform for Exploring Parallel Composition of Templates," *Technical report. arXiv preprint arXiv:1502.05347*, 2015.

[2] ——, "Parallel composition of templates for tail-energized planar hopping," in *2015 IEEE International Conference on Robotics and Automation (ICRA)*, May 2015, pp. 4562–4569.

[3] ——, "Vertical hopper compositions for preflexive and feedback-stabilized quadrupedal bounding, pacing, pronking, and trotting," *The International Journal of Robotics Research*, vol. 37, no. 7, pp. 743–778, 2018.

[4] A. M. Johnson, S. A. Burden, and D. E. Koditschek, "A hybrid systems model for simple manipulation and self-manipulation systems," *The International Journal of Robotics Research*, vol. 35, no. 11, p. 13541392, 2016.

[5] A. L. Brill, A. De, A. M. Johnson, and D. E. Koditschek, "Tail-assisted rigid and compliant legged leaping," in *Intelligent Robots and Systems (IROS), 2015 IEEE/RSJ International Conference on*. IEEE, 2015, pp. 6304–6311.

[6] M. Raibert, *Legged Robots that Balance*, ser. Artificial Intelligence. MIT Press, 1986.

[7] A. De, S. A. Burden, and D. E. Koditschek, "A hybrid dynamical extension of averaging and its application to the analysis of legged gait stability," *The International Journal of Robotics Research*, vol. 37, no. 2-3, pp. 266–286, 2018.

[8] R. J. Full and D. E. Koditschek, "Templates and anchors: neuromechanical hypotheses of legged locomotion on land," *Journal of experimental biology*, vol. 202, no. 23, pp. 3325–3332, 1999.

[9] D. C. Dunbar, "Aerial maneuvers of leaping lemurs: The physics of whole-body rotations while airborne," *American Journal of Primatology*, vol. 16, no. 4, pp. 291–303, 1988.

[10] G. A. Bartholomew and H. H. Caswell, "Locomotion in kangaroo rats and its adaptive significance," *Journal of Mammalogy*, vol. 32, no. 2, pp. 155–169, 1951.

[11] C. Walker, C. J. Vierck, and L. A. Ritz, "Balance in the cat: role of the tail and effects of sacrocaudal transection," *Behavioural Brain Research*, vol. 91, no. 1, pp. 41 – 47, 1998.

[12] E. Chang-Siu, T. Libby, M. Tomizuka, and R. J. Full, "A lizard-inspired active tail enables rapid maneuvers and dynamic stabilization in a terrestrial robot," in *2011 IEEE/RSJ International Conference on Intelligent Robots and Systems*, Sept 2011, pp. 1887–1894.

[13] G. J. Zeglin, "Uniroo–a one legged dynamic hopping robot," Ph.D. dissertation, Massachusetts Institute of Technology, 1991.

[14] T. Libby, T. Y. Moore, E. Chang-Siu, D. Li, D. J. Cohen, A. Jusufi, and R. J. Full, "Tail-assisted pitch control in lizards, robots and dinosaurs," *Nature*, vol. 481, no. 7380, pp. 181–184, Jan. 2012.

[15] A. M. Johnson, E. Chang-Siu, T. Libby, M. Tomizuka, R. J. Full, and D. E. Koditschek, "Tail assisted dynamic self righting," in *Proceedings of the International Conference on Climbing and Walking Robots*, 2012.

[16] G. Wenger, A. De, and D. E. Koditschek, "Frontal plane stabilization and hopping with a 2dof tail," in *Intelligent Robots and Systems (IROS), 2016 IEEE/RSJ International Conference on*. IEEE, 2016, pp. 567–573.

[17] P. M. Wensing, A. Wang, S. Seok, D. Otten, J. Lang, and S. Kim, "Proprioceptive Actuator Design in the MIT Cheetah: Impact Mitigation and High-Bandwidth Physical Interaction for Dynamic Legged Robots," *IEEE Transactions on Robotics*, pp. 1–14, 2017.

[18] A. De, G. Lynch, A. Johnson, and D. Koditschek, "Motor sizing for legged robots using dynamic task specification," in *2011 IEEE Conference on Technologies for Practical Robot Applications (TePRA)*, Apr. 2011, pp. 64 –69.

[19] Y. Ding and H.-W. Park, "Design and experimental implementation of a quasi-direct-drive leg for optimized jumping," 2017.

[20] E. Z. Moore, "Leg design and stair climbing control for the rhex robotic hexapod," Ph.D. dissertation, McGill University, 2002.

[21] G. Kenneally, A. De, and D. E. Koditschek, "Design Principles for a Family of Direct-Drive Legged Robots," *IEEE Robotics and Automation Letters*, vol. 1, no. 2, pp. 900–907, July 2016.

[22] X. Zhang, J. Gong, and Y. Yao, "Effects of head and tail as swinging appendages on the dynamic walking performance of a quadruped robot," *Robotica*, vol. 34, no. 12, p. 28782891, 2016.

[23] T. Libby, A. M. Johnson, E. Chang-Siu, R. J. Full, and D. E. Koditschek, "Comparative design, scaling, and control of appendages for inertial reorientation," *IEEE Transactions on Robotics*, vol. 32, no. 6, p. 13801398, 2016.

[24] A. De and D. E. Koditschek, "Averaged Anchoring of Decoupled Templates in a Tail-Energized Monoped," in *2015 International Symposium on Robotics Research*, Sept. 2015.

[25] M. T. Mason, "Compliance and force control for computer controlled manipulators," *IEEE Transactions on Systems, Man, and Cybernetics*, vol. 11, no. 6, p. 418432, 1981.

[26] T. Lozano-Perez, M. T. Mason, and R. H. Taylor, "Automatic synthesis of fine-motion strategies for robots," *The International Journal of Robotics Research*, vol. 3, no. 1, p. 324, 1984.

[27] A. De, "Modular Hopping and Running via Parallel Composition," Ph.D. dissertation, University of Pennsylvania, 2017.

[28] J. Newman, "Approximations for the bessel and struve functions," *Mathematics of Computation*, vol. 43, no. 168, pp. 551–556, 1984.

[29] "Vectornav," https://www.vectornav.com/products/vn-100.

[30] "Ghost robotics," https://www.ghostrobotics.io/.

[31] J. Seipel and P. Holmes, "Three-dimensional translational dynamics and stability of multi-legged runners," *The International Journal of Robotics Research*, vol. 25, no. 9, pp. 889–902, 2006.

[32] J. A. Grimes and J. W. Hurst, "The design of atrias 1.0 a unique monopod, hopping robot," in *Adaptive Mobile Robotics*. World Scientific, 2012, pp. 548–554.

[33] A. Abate, J. W. Hurst, and R. L. Hatton, "Mechanical Antagonism in Legged Robots." in *Robotics: Science and Systems*, 2016.

[34] A. Patel and E. Boje, "On the conical motion of a two-degree-of-freedom tail inspired by the cheetah," *IEEE Transactions on Robotics*, vol. 31, no. 6, pp. 1555–1560, Dec 2015.